Statistical analysis of observations of polar stratospheric clouds with a lidar in Kiruna, northern Sweden

Peter Voelger[1] and Peter Dalin[1]

[1]Swedish Institute of Space Physics (IRF), Kiruna, Sweden

Correspondence: Peter Voelger (peter.voelger@irf.se)

Abstract. In the present paper, we analyze 11 years of lidar measurements to derive general characteristics of Polar Stratospheric Clouds (PSCs) and to examine how mountain lee waves influence PSC properties. Measurements of PSCs were made with a backscatter lidar located in Kiruna, northern Sweden, in the lee of the Scandinavian mountain range. The statistical analysis demonstrates that nearly half of all observed PSCs consisted of nitric acid trihydrate (NAT) particles while ice clouds were only a small fraction, supercooled ternary solution (STS) and a mixture of different components making up the rest. Most PSCs were observed around 22 km altitude. Mountain lee waves provide a distinct influence on PSC chemical composition and cloud height distribution. Ice PSCs were about 5 times as frequent and NAT clouds were about half as frequent under wave conditions. PSCs were on average at 2 km higher altitudes when under the influence of mountain lee waves.

1 Introduction

Polar stratospheric clouds (PSCs) are a well-known feature of the polar wintertime stratosphere. Their influence on chemical reactions related to ozone depletion in the lower stratosphere was first postulated shortly after the discovery of the Antarctic ozone hole and has since then been subject of many studies (for reviews see e.g. Solomon (1999), Lowe and MacKenzie (2008), or Tritscher et al. (2021)). In short, PSC formation has been identified to accelerate ozone depletion by (a) enabling reactions that create chlorine radicals on the surfaces of cloud particles, (b) removing gas-phase HNO_3 in the formation of cloud particles and (c) permanently depleting the stratosphere of HNO_3 through sedimentation of those particles. The impact a PSC has on ozone concentration depends on the composition of the cloud (Kirner et al., 2015; Tritscher et al., 2021). PSCs typically consist of nitric acid trihydrate (NAT, a compound consisting of nitric acid and water at a molar ratio of 1:3), supercooled ternary solution (STS, a mixture of nitric acid, sulfuric acid and water), or water ice. In the context of lidar measurements such clouds are also referred to as type Ia, Ib and II, respectively (Browell et al., 1990), as the backscatter signals from these different PSC types have very distinct characteristics. Additional subtypes have been proposed to explain observations that don't fit any of the above three types. These subtypes include modified components or mixtures of the basic cloud types (see e.g. Tabazadeh and Toon (1996), Stein et al. (1999), Massoli et al. (2006)). Based on laboratory studies additional compounds have been predicted to exist in PSCs but could, so far, not be identified in natural stratospheric clouds beyond any doubt (Tritscher et al. (2021) and references therein).

25   The significant contribution of PSCs to ozone depletion is one of the major reasons for investigating and monitoring these clouds. Satellites, due to the near global coverage of their observations, offer a way to study the worldwide distribution of PSCs. An early attempt to prepare a multiyear statistic based on satellite data was undertaken by Poole and Pitts (1994) who statistically analysed PSC occurence by means of limb measurements with the photometer SAM II on board of Nimbus 7. Datasets from other, more advanced instruments have become available in recent decades. Prominent examples are MIPAS

30   (Michelson Interferometer for Passive Atmospheric Sounding) on board of Envisat (2002–2012) and CALIOP (Cloud-Aerosol Lidar with Orthogonal Polarization) on the Calipso satellite (since 2006). On the basis of MIPAS measurements it was possible to infer the chemical composition of clouds. The MIPAS dataset has been utilised for long-term studies of the composition of PSCs (Spang et al., 2018). CALIOP collects backscatter signals from the atmosphere that give information about PSCs with better spatial resolution than what is possible with passive remote sensing techniques. The data has resulted in estimates of the

35   global distribution of PSCs (see e.g. Pitts et al., 2018).

       While satellite-borne instruments provide observations with nearly global coverage, ground-based lidar measurements are better suited to give insight in how the specific conditions at the location of the instrument affect PSCs. The time and vertical resolution of ground-based lidar observations are better than what can be achieved by spaceborne instruments, thus enabling detailed studies of local pecularities. Several ground-based lidars have been or were operating over sufficiently long periods

40   to allow for the statistical analysis of PSC characteristics at the respective locations. Santacesaria et al. (2001) compiled such data for the lidar at the Dumont d'Urville research station in Antarctica, Adriani et al. (2004) published a similar survey for the McMurdo station, also in Antarctica. Studies for data from the Arctic region were published by Massoli et al. (2006) for Ny-Ålesund, Spitsbergen, and by Blum et al. (2005) and Achtert and Tesche (2014), both the latter examined more than a decade of measurements with a lidar at Esrange in northern Sweden.

45   Atmospheric waves are known to create temperature pertubation due to adiabatic cooling/warming when a wave forces an air parcel to move vertically. In the stratosphere such changes of the temperature can affect PSC formation and composition. As most prominent sources for waves have been identified topography, convection and adjustment of unbalanced flow near jet streams and frontal systems (Hoffmann et al., 2017). Depending on the horizontal wavelength atmospheric waves are classified as planetary, synoptic-scale, or gravity waves. Of the latter type, inertia gravity waves are significant, since they are

50   not trapped at low altitudes but can propagate up to the stratosphere (Fritts and Alexander, 2003). Utilizing ECMWF analysis data Teitelbaum and Sadourny (1998) showed that the distribution of temperatures that allow the formation of PSCs in the Arctic region is, to a large extent, correlated with the upwelling of isentropic surfaces as a result of planetary waves. Kohma and Sato (2011) used, among other data sets, CALIPSO observations to examine the extent to which waves of different scales influence the formation of PSCs. They deduced that stationary planetary waves are the dominant factor in the formation of

55   PSCs in the Arctic while synoptic-scale waves only have small influence. They further concluded that inertia gravity waves have negligible impact on Arctic PSC formation. Their reasoning, however, is based on data from only one winter season which, given the large interannual variability of Arctic winter conditions, is a too short period to draw definite conclusions. On the other hand, Alexander et al. (2013), using CALIPSO and other satellite data spanning four winter seasons, determined that mountain lee waves, a subtype of inertia gravity waves, significantly influenced PSC composition and were responsible for

60   nearly 1/3 of all PSC occurences in the Arctic. The differences between the conclusions by Kohma and Sato (2011) and those
       by Alexander et al. (2013) indicate that, due to large interannual variability, statistically sound conclusions have to be based on
       a data base that spans several years or more.

       Mountain lee waves are typically generated when air is vertically displaced while wind is blowing across mountains. Under
       favourable conditions such waves can propagate from the surface up to the mesosphere. The stratospheric temperature pertuba-
65   tions that are associated with them can be as much as 10 degrees or more (Dörnbrack et al., 1997). Hence, they can trigger both
       the formation of a PSC (Voelger and Dalin, 2021) and the change of the cloud composition (Carslaw et al., 1999). Although
       mountain lee waves are regionally confined phenomena they can set off the formation of meso-scale PSCs (Carslaw et al.,
       1998; Eckermann et al., 2009). Hence, they can cause large-scale ozone depletion. Pitts et al. (2011) showed that CALIPSO
       data can be used to detect the impact of mountain lee waves on PSCs and Alexander et al. (2013) utilised this capability for
70   estimating the role of these waves in PSC formation. However, Alexander et al. (2013) pointed out that CALIPSO can miss the
       detection of mountain lee waves, as only a small, random portion of a wave might be sampled which not necessarily shows the
       backscatter characteristics which were defined for identifying waves in CALIPSO observations. Moreover, the low sampling
       frequency results in that many cases with waves being present are missed. For fixed locations observations with a groundbased
       lidar can therefore give more detailed data.

75   Kiruna, the location of our lidar, is situated on eastern slopes of the northern part of the Scandinavian mountain range, a
       region where mountain lee waves frequently occur (Rao et al., 2008). Several field campaigns have been conducted in northern
       Scandinavia in the past decades which investigated cases when mountain lee waves influenced composition and geometry of
       PSCs (see e.g. Tsias et al., 1999; Dörnbrack et al., 2002). The aim of our study is to present a systematic investigation of
       the impact mountain lee waves have on PSC characteristics at a location where such waves are frequently present. We will
80   use data from 11 years of measurements with our lidar (in the following also referred to as *IRF lidar*) both to derive general
       characteristics of the observed PSCs and to examine how mountain lee waves influence PSC properties. We first shortly describe
       the lidar and the data that has been used in this study. We then derive some general characteristics of PSCs over our location
       and compare them with results from similar studies. Thereafter we discuss, with help of a statistical analysis of the data, how
       mountain lee waves modified PSCs above Kiruna.

85   2   Tools

       Lidar observations were performed with a backscatter lidar that is located on the premises of the Swedish Institute of Space
       Physics (IRF) in Kiruna at $67.84°$N, $20.41°$E. The lidar operates at 532 nm wavelength and has two detection channels to dis-
       tinguish backscatter signals with two orthogonal planes of polarisation. Light with the same plane of polarisation as the laser
       will in the following be denoted as parallel while perpendicular will refer to light with a polarisation plane perpendicular to
90   that of the laser. Height and time resolution are 30 m and 133 s, respectively. The altitude range for observations is from 5 to 50
       km (see Voelger and Nikulin (2005) for a more detailed description of the lidar characteristics). Measurements were performed
       during winters from 2007/08 to 2017/18 whenever conditions were favourable for the presence of PSCs, i.e. predicted temper-

atures in the stratosphere were approximately around PSC existence temperatures or lower, and weather conditions allowed for lidar measurements of the stratosphere. Temperature predictions were provided by the Danish Meteorological Institute, based on forecasts by the European Centre for Medium-Range Forecast (ECMWF). Lidar observations were restricted to nighttime and twilight for better signal quality. For the subsequent analysis we integrated our measurement data over time to derive hourly averages. Additionally, a 5-point moving average over altitude was applied.

The signal that the lidar detects is proportional to the backscattering that is caused by molecules, aerosol particles and cloud particles in the atmosphere. When considering the stratosphere the contribution of particles to the backscattering at 532 nm from a cloud-free atmosphere (i.e. outside PSCs) can be assumed to be a few percent only (Thomason et al., 2007). In the context of PSC observations the backscattering from both molecules and aerosol particles combined represent the background signal.

Parameters that are commonly used to describe PSCs in lidar measurements are the backscatter ratio of the parallel channel, $R_{\parallel}$, and the depolarisation ratio δ. We define $R_{\parallel}$ as the ratio of total backscatter coefficient to that of the atmospheric background, both for the parallel channel:

$$R_{\parallel} = \frac{\beta_{\parallel,PSC} + \beta_{\parallel,BG}}{\beta_{\parallel,BG}} \tag{1}$$

with β being the backscatter coefficient and indices PSC and BG denoting cloud and background, respectively. As background we consider contributions from both molecules and stratospheric aerosol particles. R is larger than 1 implies that a cloud is present. The backscatter coefficient of the background can be assumed to be proportional to the interpolated signals from below and above the PSC. Similarly, the cumulative backscatter coefficients of background and PSCs is proportional to the total backscatter signal. Hence, $R_{\parallel}$ can be calculated as

$$R_{\parallel} = \frac{I_{\parallel,tot}}{I_{\parallel,BG}} \tag{2}$$

where $I_{\parallel,tot}$ denotes the total backscatter signal and $I_{\parallel,BG}$ the interpolated signal without PSC, both for the parallel channel. The backscatter ratio for the perpendicular channel, $R_{\perp}$, can be estimated in an analogous way. From the backscatter ratios for both channels the depolarisation ratio can be determined:

$$\delta = \frac{R_{\perp}}{R_{\parallel}} \delta_{mol} \tag{3}$$

where δ_{mol} is the depolarisation ratio of molecular backscattering. We assume that stratospheric background aerosol particles are predominantly sulfuric acid droplets which are spherical particles and, therefore, do not change the polarisation of light that is scattered on them at $180°$ (i.e. backscattering). For our lidar we estimate δ_{mol} as 0.02. The backscatter signals in both receiver channels can be skewed by (a) cross talk between both channels and (b) polarising effects of the receiver optics. We examined the error from both sources by using white light with a controlled state of polarisation (method described by Mattis et al. (2009)). Our tests showed that the errors for our lidar are negligible.

For evaluation of the atmospheric conditions that were prevalent during lidar measurements we used horizontal wind fields from the ERA5 dataset that can be obtained from ECMWF (Hersbach et al., 2020). Such data is available for every full hour

125 with a horizontal resolution of 31 km. The data comes at 137 vertical levels between surface and 1 Pa pressure level since mid 2013 and at 91 levels before.

3 Data analysis

3.1 General PSC characteristics

The lidar was operated during 11 winter seasons, starting in late 2007 and ending in early 2018. During this period mea-
130 surements of PSCs were performed in 102 nights. In total, 738 hours of observations were accumulated. The distribution of measurement times per year is shown in Figure 1. The number of nights with observations per season was varying between 2 nights during winter 2014/15 and 19 nights (2015/16). The year-to-year variation is partly due to interannual variations of the polar vortex, as has been discussed for CALIPSO data by Pitts et al. (2018). Another limiting factor are tropospheric clouds that, if they are optically too thick, prohibit measurements of stratospheric features from the ground. More than half of all
135 PSC events were observed during January. The earliest measurement during a winter season was on November, 30th (2017), the latest on February 18th (2017). In all years considered here, PSCs were visible by eye more often than conditions were sufficiently good to perform lidar measurements.
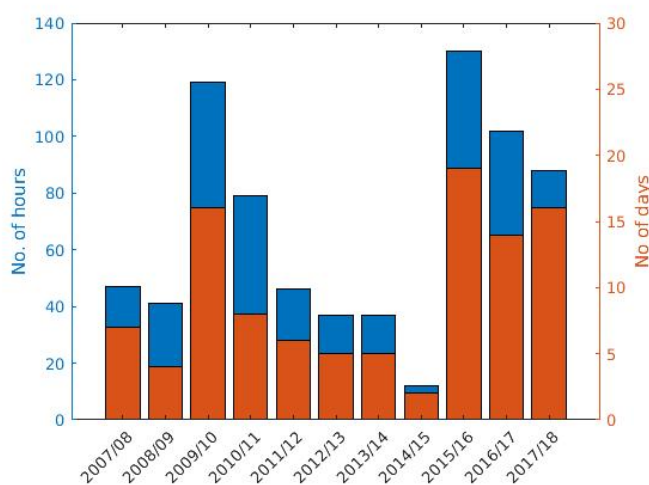
Figure 1. Annual statistic of IRF lidar measurements. Blue marks the hours of measurements per year, red bars are the number of nights with PSC observations.

Hourly averages were calculated for all available measurement data and included in the following analysis. In their study of PSCs at the McMurdo station Adriani et al. (2004) utilised only one profile per Julian day in order to avoid a possible bias
140 when observation periods vary from day to day. This approach presumes that PSCs show only minor variations during a day so that one hourly profile can be considered as representative for the whole 24 hour period. As mountain lee waves are frequently

PSC type		Backscatter ratio $R_{\parallel}$	Depolarisation ratio δ
Type Ia (NAT)		$1.05 < R_{\parallel} < 2$	$\delta > 10\%$
Type Ib (STS)		$1.1 < R_{\parallel} < 5$	$\delta < 2\%$
Type II (ice)	either	$2 < R_{\parallel} < 7$	$\delta > 3\%$
	or	$R_{\parallel} > 7$	any

Table 1. Classification criteria for PSCs observed with the IRF lidar.

present at our location, PSC characteristics can change significantly within short time. Using only one profile per Julian day would not account for the variations that occured during that period, or, in our case, over the course of a night.

The characteristics of the backscatter signal from a PSC depend on the type of particles in the cloud. Combining signal
145 strength, or as a derived parameter, the backscatter ratio, with the depolarisation of the backscatter makes it possible to classify PSCs according to their composition. However, parameter ranges depend in part on the lidar system and the wavelength(s) it utilises. Several sets of criteria to classify observed clouds have been suggested in the past (see e.g. Browell et al., 1990; Biele et al., 2001; Pitts et al., 2018). Achtert and Tesche (2014) compared a selection of classification schemes and concluded that the decision which scheme is most suitable depends on the type of data that is available.

150 Our classification is similar to the one suggested by Blum et al. (2005), as both our lidar setup as well as the format of our data is similar to theirs. For the backscattered signal to be interpreted as being influenced by the presence of PSCs the backscatter ratios in either detection channel should be clearly distinguishable from the background. For our lidar data we set lower limits to 1.05 and 1.1 for the parallel and the perpendicular channel, respectively. These numbers mean that we potentially miss a few very thin PSCs. However, in the vast number of cases cloud boundaries were not sensitive to the lower limits for R. The values
155 used in our classification scheme are summarised in Table 1. Combinations of $R_{\parallel}$ and δ that don't match any particular PSC type are assumed to consist of a mixture of different types of particles. It has to be noted that PSCs that are classed as a certain type can contain some, minor amount of other compound as well (Biele et al., 2001; Pitts et al., 2009).

Figure 2 shows a 2-D histogram of the backscatter ratios for parallel and perpendicular polarisation for cloud increments of all our measurements. Two regions with large numbers of observations become obvious, one with small $R_{\parallel}$ and large $R_{\perp}$ (i.e.
160 large δ), as characteristic for type Ia, and one vice versa (type Ib). Additionally, the histogram shows a cluster of measurements with large R in both channels, indicating type II PSCs.

Displaying all our measurements as a piechart (Figure 3) shows that PSCs of type Ia were most common with almost half of all measurement points (46%). Type II amounted to 6% of the observations while Ib and a mixture of particles occured in 26% and 21% of all cases, respectively. The large portion of type Ia clouds can be attributed to the fact that STS and ice
165 particles require lower stratospheric temperatures to exist which often are not reached in the Arctic stratosphere. Compared to Pitts et al. (2018) our data shows less NAT PSCs and more mixed-type clouds. A possible reason could be that Pitts et al.
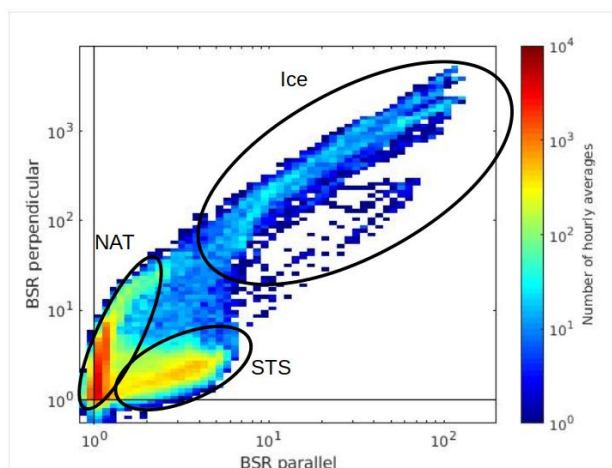
Figure 2. Frequency of backscatter ratios of parallel versus perpendicular channel for all PSC observations with the IRF lidar. Typical parameter ranges for PSC types Ia, Ib, and II are indicated.

(2018) included data for the whole Arctic region while ours are from a single location. In comparison to Blum et al. (2005) our data contains more observations of NAT and less STS clouds. Differences could be due to their measurements being performed during campaigns, mostly between end of December and end of January when the Arctic polar vortex often is in its coldest

170 phase. Our measurements, on the other hand, were done throughout the whole PSC season. Therefore, they were more often covering periods when the polar vortex was less well developed and, hence, the stratosphere was relatively warm.

The height distribution of our PSC observations is shown in Figure 4. For statistical purposes all cloud pixels were integrated into 1 km height intervals. The lowest clouds were observed between 14 and 15 km, the highest were between 33 and 34 km (The number of cloud pixels in the highest interval was too small to be distinguished from the y-axis of the Figure 4.). Most

175 frequent occurences were at altitudes of 21 to 23 km. This is consistent with findings by Pitts et al. (2018) for the Arctic region as the whole. In all cases when cirrus clouds were present during measurements they were spatially separated from the lowest PSC layer by at least a few km. Hence, an erroneous classification of a cirrus cloud as PSC can be excluded for our data. The relative frequency of cloud types differed with altitude and is presented in Figure 5. Type Ia clouds were prevalent up to 26 km while above a mixture of particle types was more common. Type II clouds were rarely observed below 20 km but most

180 common between 28 and 30 km. Given the different existence temperatures for PSC types this suggests that PSCs at higher altitudes are more likely to have relatively low temperatures.

3.2 Wave influence on PSCs

The Scandinavian mountain range is known to be one of the major sources for mountain lee waves in the Arctic region (Hoffmann et al., 2017). This circumstance has triggered several case studies, addressing the questions related to the generation
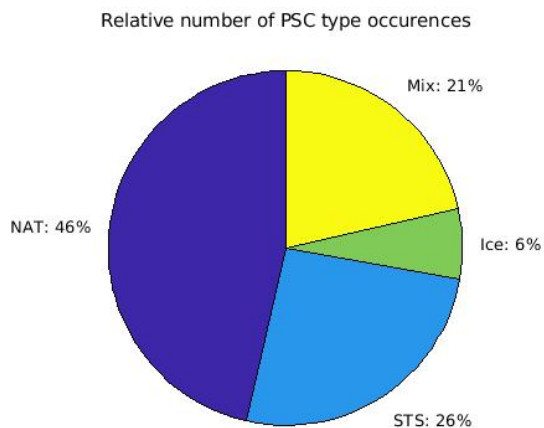
Figure 3. Relative distribution of PSC types for all measurements.
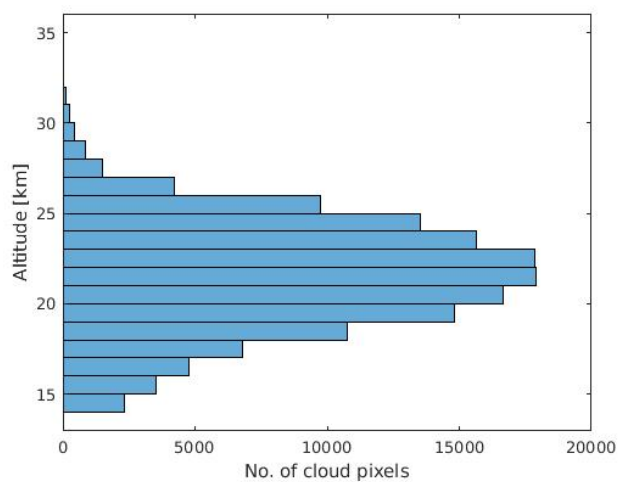
Figure 4. Height distribution of detected PSCs.
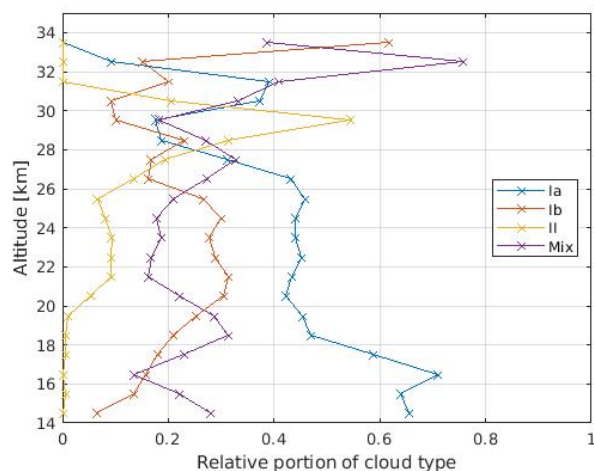
Figure 5. Relative portions of PSC types as function of altitude.

of waves in northern Scandinavia and how they affect the atmosphere, in particular, the formation of PSCs (see e.g. Tsias et al. (1999) and Dörnbrack et al. (2002)). For such waves to be propagating from the lower troposphere up to the stratosphere certain meteorological conditions need to be fulfilled. Dörnbrack et al. (2001) summarised them as follows:

1. The horizontal wind speed at 900 hPa has to be larger than a threshold value: $v_{hor}(900hPa) > v_{crit}$.

2. The direction of the horizontal wind at 900 hPa, $\alpha_{hor}(900hPa)$, must be approximately perpendicular to the mountain ridge: $\alpha_{mnt} - \Delta\alpha < \alpha_{hor}(900hPa) < \alpha_{mnt} + \Delta\alpha$.

3. The wind direction at higher altitudes (pressure levels) doesn't differ much from that at 900 hPa: $\Delta\alpha(p) = \alpha_{hor}(p) - \alpha_{hor}(900hPa) < \Delta\alpha$, with $p = 500, 300, 100, 50$ hPa.

In the case of the Scandinavian mountain range the orientation of the ridge in northern Scandinavia is from NNE to SSW at an angle of about $30°$ clockwise to the direct north. Hence, the wind direction perpendicular to the mountain range is $\alpha_{mnt} = 300°$. However, since the mountain range is not perfectly aligned even wind directions that are off the nominal normal by a certain angle α_{hor} can still lead to lee waves. We set the thresholds to $\Delta\alpha = 45°$ and $v_{crit} = 10m/s$, the same value as suggested by Dörnbrack et al. (2001).

Wind data were obtained from ECMWF's ERA5 dataset. A combination of all three criteria was applied to identify PSC measurements that were influenced by mountain lee waves. Figure 6 shows the year-to-year distribution of observation hours, divided into those with conditions that allowed mountain lee waves to propagate to the stratosphere and those that did not. Accumulated over the whole period, 230 hours of measurements were with mountain lee waves present, whereas 508 hours were without such waves. However, there is a strong interannual variability, both in total measurements and the portion of them that were influenced by waves. The latter can be attributed to the fact that the year-to-year variations of the troposphere result

in that the chances for conditions to develop that are favourable for gravity waves differ largely over the years, as well. Reasons for the variation of the total observation time were discussed further above.
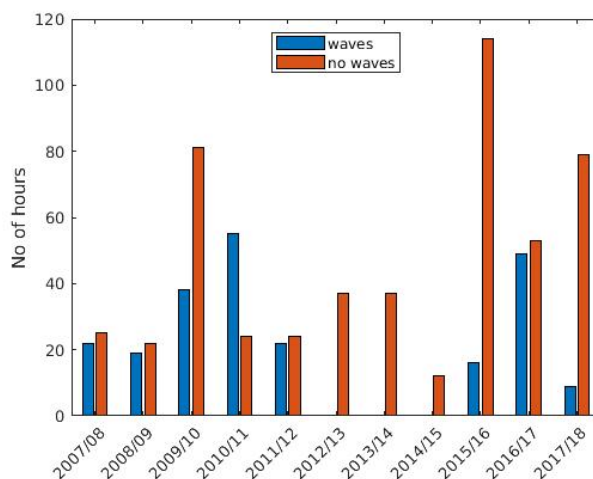
Figure 6. Annual statistic of hours of measurements with the IRF lidar. Blue bars mark times with conditions favourable for mountain lee waves based on criteria established by Dörnbrack et al. (2001), red bars are all other instances.

205

It has to be noted that inertia gravity waves can also be due to reasons other than topography, such as wind shears and wind jets which are caused by tropospheric pressure systems and the polar jet stream. Just as mountain lee waves, the temperature pertubations that they trigger can contribute to the modification or formation of PSCs (Hitchman et al., 2003; Shibata et al., 2003). However, the sources for these waves are not specific for our location but can also be found in other parts of the polar

210 regions. Therefore, the impact of non-orographic waves is not subject of this study.

The separation of wave and nonwave cases leads to two very different distributions of observed backscatter ratios. A significant portion of observations during wave conditions had a combination of large numbers of backscatter ratios for both states of polarisation, a manifestation of the presence of ice particles (Figure 7b). Such observations were absent for measurements that were not influenced by mountain lee waves (Figure 7a). Apparently, the presence of waves was a precondition for the formation

215 of PSCs that yield such backscatter ratios at our location in northern Scandinavia. Visualising the portions of different PSC types as a pie chart for conditions with and without mountain lee waves separately confirms that relative occurences of these types are notably different for both atmospheric conditions (Figure 8). In the case of no waves present type Ia clouds made up the majority of all measurements (53%), while type II was rarely observed (3%). This agrees well with findings by Pitts et al. (2018) for the whole set of CALIPSO measurements of the Arctic region for an 11-year period. On the other hand, when

220 conditions for mountain lee waves were favourable, type Ia, Ib and mixed clouds were observed at approximately the same frequency. Type II clouds were more common and stood for about 1/6 off all measurements. Hence, mountain lee waves can locally cause very different distribution of cloud types. A consequence is that ozone chemistry is affected by PSCs in regionally different ways. An investigation of such effects, however, is beyond the scope of this study.
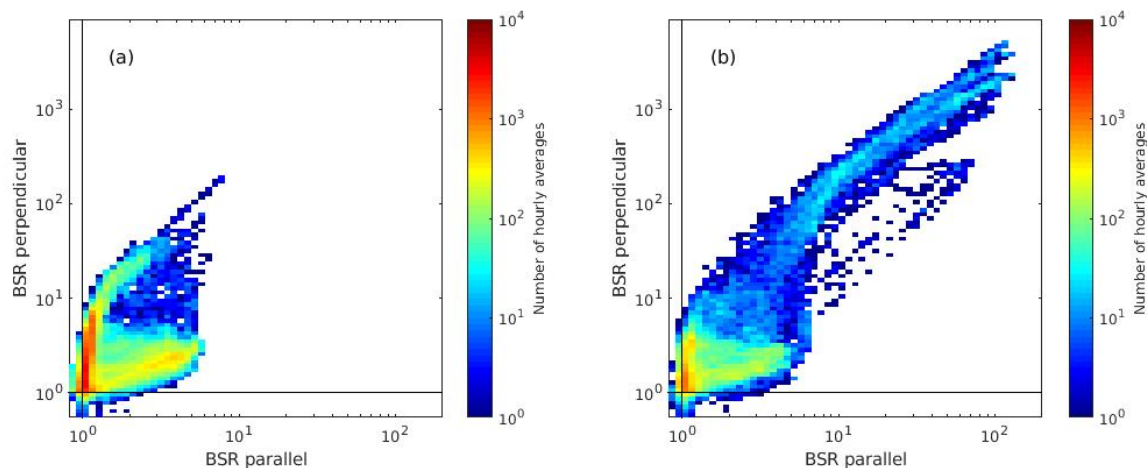
Figure 7. Frequency of backscatter ratios of parallel versus perpendicular channel for PSC observations (a) in the absence of mountain lee waves and (b) when waves could propagate to the stratosphere.

Another consequence of the influence of mountain lee waves is a change of the altitude of PSCs. Figure 9 shows the altitude
225 distributions of observed clouds, separated for cases with influence of mountain lee waves (right panel) and without (left panel). Apparently, in the presence of mountain lee waves, the maximum number of the cloud observations was moved to larger heights by 2 to 3 km. Cloud bottoms and tops show a similar change, indicating that cloud layers as a whole shifted to larger heights.

The polar stratosphere has been cooling over the last decades which, based on simulations with global circulation models, is expected to continue in the foreseeable future (Fleming et al., 2011). This, in turn, will result in an increase of PSC occurences
230 (Rex et al., 2004; von der Gathen et al., 2021). The period of measurements that is discussed here is however too short to deduce any statistically significant trend over time.

4   Summary

Measurements of PSCs with a backscatter lidar in Kiruna, northern Sweden, were analysed. The data comprises 11 winter seasons, a period sufficiently long to allow for a statistical analysis. Nearly half of all observed clouds consisted of NAT
235 particles while ice clouds were only a small fraction, STS and a mixture of different components making up the rest. The most common altitude for observed PSCs was around 22 km. Those results are in agreement with findings by Pitts et al. (2018) and Blum et al. (2005). When separating lidar observations that were influenced by mountain lee waves and those without such waves present, clearly distinct characteristics become apparent. Ice PSCs (type II) were about 5 times as frequent during wave conditions. On the other hand, NAT clouds (type Ia) were about half as frequent under wave conditions than without mountain
240 lee waves being present. Observed PSCs were, on average, at 2 km higher altitudes when under the influence of mountain lee waves.
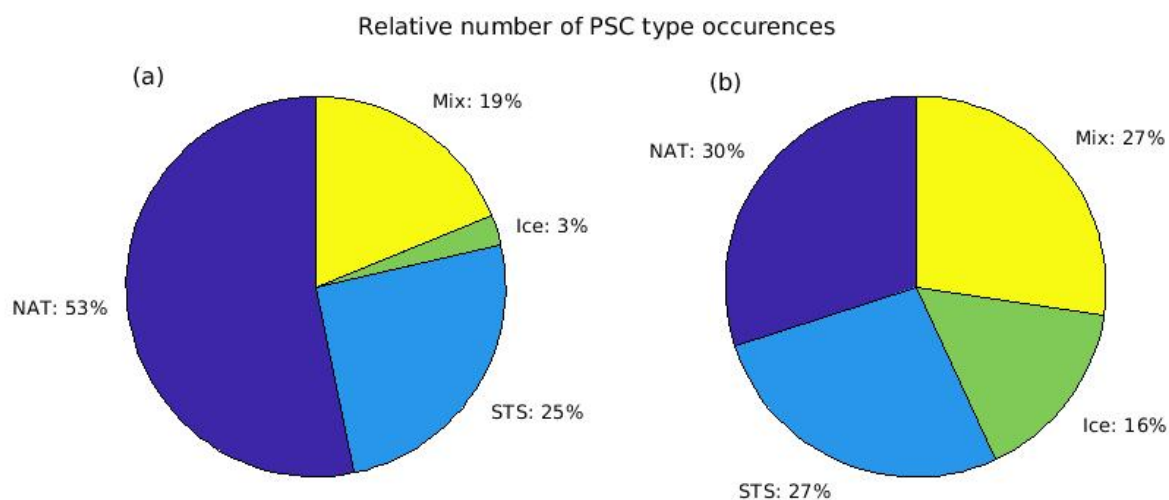
Figure 8. Relative distribution of PSC observations (a) in the absence of mountain lee waves and (b) when waves could propagate to the stratosphere (right).
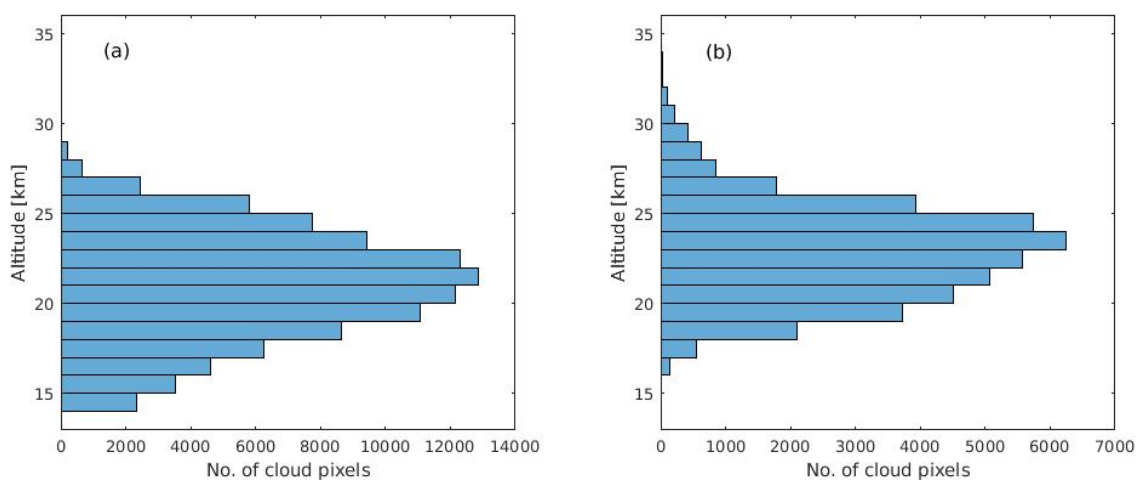
Figure 9. Height distribution of PSC observations (a) in the absence of mountain lee waves and (b) when waves could propagate to the stratosphere.

Data availability. Lidar data is available from the authors on request. ERA5 datasets can be obtained by approved users from ECMWF (http://www.ecmwf.int).

Author contributions. PV and PD performed lidar observations and inverted measurement data. PV did the statistical analysis. PV prepared the manuscript with contributions from PD.

Competing interests. The authors declare that they have no conflict of interest.

Acknowledgements. We thank the Danish Meteorological Institute for providing PSC and vortex forecasts. We greatfully acknowledge Daria Mikhaylova (IRF) for invaluable help with lidar operations and Oliver Willbrink (Luleå University of Technology, Sweden) for an initial assessment of lidar observation data. We also thank Ronny Engelmann (Leibniz Institute for Tropospheric Research, Germany) for kindly providing instrumentation for testing receiver channel performance.

References

Achtert, P. and Tesche, M.: Assessing lidar-based classification schemes for polar stratospheric clouds based on 16 years of measurements at Esrange, Sweden, J. Geophys. Res., 119, 1386–1405, https://doi.org/10.1002/2013JD020355, 2014.

Adriani, A., Massoli, P., Donfrancesco, G. D., Cairo, F., Moriconi, M. L., and Snels, M.: Climatology of polar stratospheric clouds based on lidar observations from 1993 to 2001 over McMurdo Station, Antarctica, J. Geophys. Res., 109, D24 211–1–D24 211–17, https://doi.org/10.1029/2004JD004800, 2004.

Alexander, S. P., Klekociuk, A. R., McDonald, A. J., and Pitts, M. C.: Quantifying the role of orographic gravity waves on polar stratospheric cloud occurrence in the Antarctic and the Arctic, J. Geophys. Res., 118, 11 493–11 507, https://doi.org/10.1002/2013JD020122, 2013.

Biele, J., Tsias, A., Luo, B. P., Carslaw, K. S., Neuber, R., Beyerle, G., and Peter, T.: Nonequilibrium coexistence of solid and liquid particles in Arctic stratospheric clouds, J. Geophys. Res., 106, 22 991–23 007, https://doi.org/10.1029/2001JD900188, 2001.

Blum, U., Fricke, K. H., Müller, K. P., Siebert, J., and Baumgarten, G.: Long-term lidar observations of polar stratospheric clouds at Esrange in northern Sweden, Tellus B, 57, 412–422, https://doi.org/10.3402/tellusb.v57i5.16562, 2005.

Browell, E. V., Butler, C. F., Ismail, S., Robinette, P. A., Carter, A. F., Higdon, N. S., Toon, O. B., Schoeberl, M. R., and Tuck, A. F.: Airborne lidar obsevations in the wintertime arctic stratosphere: polar stratospheric clouds, Geophys. Res. Lett., 17, 385–388, https://doi.org/10.1029/GL017i004p00385, 1990.

Carslaw, K. S., Wirth, M., Tsias, A., Luo, B. P., Dörnbrack, A., Leutbecher, M., Volkert, H., Renger, W., Bacmeister, J. T., Reimer, E., and Peter, T.: Increased stratospheric ozone depletion due to mountain-induced atmospheric waves, Nature, 391, 675–678, https://doi.org/10.1038/35589, 1998.

Carslaw, K. S., Peter, T., Bacmeister, J. T., and Eckermann, S. D.: Widespread solid particle fomration by mountain waves in the Arctic stratosphere, J. Geophys. Res., 104, 1827–1836, https://doi.org/10.1029/1998JD100033, 1999.

Dörnbrack, A., Leutbecher, M., Volkert, H., and Wirth, M.: Mesoscale forecasts of stratospheric mountain waves, Meteorol. Appl., 5, 117–126, https://doi.org/10.1017/S1350482798000802, 1997.

Dörnbrack, A., Leutbecher, M., Reichardt, J., Behrendt, A., Müller, K.-P., and Baumgarten, G.: Relevance of mountain wave cooling for the formation of polar stratospheric clouds over Scandinavia: Mesoscale dynamics and observations for January 1997, J. Geophys. Res., 106, 1569–1581, https://doi.org/10.1029/2000JD900194, 2001.

Dörnbrack, A., Birner, T., Fix, A., Flentje, H., Meister, A., Schmid, H., Browell, E. V., and Mahoney, M. J.: Evidence for inertia gravity waves forming polar stratospheric clouds over Scandinavia, J. Geophys. Res., 107, SOL30, https://doi.org/10.1029/2001JD000452, 2002.

Eckermann, S. D., Hoffmann, L., Höpfner, M., Wu, D. L., and Alexander, M. J.: Antarctic NAT PSC belt of June 2003: Observational validation of the mountain wave seeding hypothesis, Geophys. Res. Lett., 36, L02 807, https://doi.org/10.1029/2008GL036629, 2009.

Fleming, E. L., Jackman, C. H., Stolarski, R. S., and Douglass, A. R.: A model study of the impact of source gas changes on the stratosphere for 1850–2100, Atm. Chem. Phys., 11, 8515–8541, https://doi.org/10.5194/acp-11-8515-2011, 2011.

Fritts, D. C. and Alexander, M. J.: Gravity wave dynamics and effects in the middle atmosphere, Rev. Geophys., 41, 1003, https://doi.org/10.1029/2001RG000106, 2003.

Hersbach, H., Bell, B., Berrisford, P., Hirahara, S., Horányi, A., Munoz-Sabater, J., Nicolas, J., Peubey, C., Radu, R., Schepers, D., Simmons, A., Soci, C., Abdalla, S., Abellan, X., Balsamo, G., Bechtold, P., Biavati, G., Bidlot, J., Bonavita, M., Chiara, G. D., Dahlgren, P., Dee, D., Diamantakis, M., Dragani, R., Flemming, J., Forbes, R., Fuentes, M., Geer, A., Haimberger, L., Healy, S., Hogan, R. J., Hólm, E.,

Janisková, M., Keeley, S., Laloyaux, P., Lopez, P., Vamborg, C., Villaume, S., and Thépaut, J.-N.: The ERA5 global reanalysis, Quart. J. Roy. Meteorol. Soc., 146, 1999–2049, https://doi.org/10.1002/qj.3803, 2020.

Hitchman, M. H., Buker, M. L., Tripoli, G. J., Browell, E. V., Grant, W. B., McGee, T. J., and Burris, J. F.: Nonorographic generation of Arctic polar stratospheric clouds during December 1999, J. Geophys. Res., 108, 8325, https://doi.org/10.29/2001JD001034, 2003.

Hoffmann, L., Spang, R., Orr, A., Alexander, M. J., Holt, L. A., and Stein, O.: A decadal satellite record of gravity wave activity in the lower stratosphere to study polar stratospheric cloud formation, Atm. Chem. Phys., 17, 2901–2920, https://doi.org/10.5194/acp-17-2901-2017, 2017.

Kirner, O., Müller, R., Ruhnke, R., and Fischer, H.: Contribution of liquid, NAT and ice particles to chlorine activation and ozone depletion in Antarctic winter and spring, Atm. Chem. Phys., 15, 2019–2030, https://doi.org/10.5194/acp-15-2019-2015, 2015.

Kohma, M. and Sato, K.: The effects of atmospheric waves on the amount of polar stratospheric clouds, Atm. Chem. Phys., 11, 11 535–11 552, https://doi.org/10.5194/acp-11-11535-2011, 2011.

Lowe, D. and MacKenzie, A. R.: Polar straospheric cloud microphysics and chemistry, J. Atmos. Solar-Terr. Phys., 70, 13–40, https://doi.org/10.1016/j.jastp.2007.09.011, 2008.

Massoli, P., Maturilli, M., and Neuber, R.: Climatology of Arctic polar stratospheric clouds as measured by lidar in Ny-Ålesund, Spitsbergen (79°N, 12°E, J. Geophys. Res., 111, D09 206, https://doi.org/0.1029/2005JD005840, 2006.

Mattis, I., Tesche, M., Grein, M., Freudenthaler, V., and Müller, D.: Systematic error of lidar profiles caused by a polarization-dependent receiver transmission: quantification and error correction scheme, Appl. Opt., 48, 2742–2751, https://doi.org/10.1364/AO.48.002742, 2009.

Pitts, M. C., Poole, L. R., and Thomason, L. W.: CALIPSO polar stratospheric cloud observations: second-generation detection algorithm and composition discrimination, Atm. Chem. Phys., 9, 7577–7589, https://doi.org/10.5194/acp-9-7577-2009, 2009.

Pitts, M. C., Poole, L. R., Dörnbrack, A., and Thomason, L. W.: The 2009–2010 Arctic polar stratospheric cloud season: a CALIPSO perspective, Atm. Chem. Phys., 11, 2161–2177, https://doi.org/10.5194/acp-11-2161-2011, 2011.

Pitts, M. C., poole, L. R., and Gonzalez, R.: Polar stratospheric cloud climatology based on CALIPSO spaceborne lidar measurements from 2006 to 2017, Atm. Chem. Phys., 18, 10 881–10 913, https://doi.org/10.5194/acp-18-10881-2018, 2018.

Poole, L. R. and Pitts, M. C.: Polar straospheric cloud climatology based on Stratospheric Aerosol Measurement II observations from 1978 to 1989, J. Geophys. Res., 99, 13 083–13 089, https://doi.org/10.1029/94JD00411, 1994.

Rao, T. N., Arvelius, J., and Kirkwood, S.: Climatology of tropopause folds over a European Arctic station (Esrange), J. Geophys. Res., 113, D00B03, https://doi.org/10.1029/2007JD009638, 2008.

Rex, M., Salawitch, R. J., von der Gathen, P., Harris, N. R. P., Chipperfield, M. P., and Naujokat, B.: Arctic ozone loss and climate change, Geophys. Res. Lett., 31, L04 116, https://doi.org/10.1029/2003GL018844, 2004.

Santacesaria, V., McKenzie, A. R., and Stefanutti, L.: A climatological study of polar stratospheric clouds (1989–1997) from LIDAR measurements over Dumont d'Urville (Antarctica), Tellus B, 53B, 306–321, https://doi.org/10.1034/j.1600-0889.2001.01155.x, 2001.

Shibata, T., Sato, K., Kobayashi, H., Yabuki, M., and Shiobara, M.: Antarctic polar stratospheric clouds under temperature perturbation by nonorographic inertia gravity waves observed by micropulse lidar at Syowa Station, J. Geophys. Res., 108, ACC 6, https://doi.org/0.1029/2002JD002713, 2003.

Solomon, S.: Stratospheric ozone depletion: a review of concepts and history, Rev. Geophys., 37, 275–316, https://doi.org/10.1029/1999RG900008, 1999.

Spang, R., Hoffmann, L., Müller, R., Groß, J.-U., Tritscher, I., Höpfner, M., Pitts, M., Orr, A., and Riese, M.: A climatology of polar
    stratospheric cloud composition between 2002 and 2012 based on MIPAS/Envisat observations, Atm. Chem. Phys., 18, 5089–5113,
    https://doi.org/10.5194/acp-18-5089-2018, 2018.

Stein, B., Wedekind, C., Wille, H., Immler, F., Müller, M., Wöste, L., del Guasta, M., Morandi, M., Stefanutti, L., Antonelli, A., Agostini,
    P., Rizi, V., Readelli, G., Mitev, V., Matthey, R., Kivi, R., and Kyrö, E.: Optical classification, existence temperature, and coexistence of
    different polar stratospheric cloud types, J. Geophys. Res., 104, 23 983–23 993, https://doi.org/10.1029/1999JD900064, 1999.

Tabazadeh, A. and Toon, O. B.: The presence of metastable HNO_3/H_2O solid phases in the stratosphere inferred from ER 2 data, J.
    Geophys. Res., 101, 9071–9078, https://doi.org/10.1029/96JD00062, 1996.

Teitelbaum, H. and Sadourny, R.: The rôle of planetary waves in the formation of polar stratospheric clouds, Tellus, 50A, 302–312,
    https://doi.org/10.3402/tellusa.v50i3.14528, 1998.

Thomason, L. W., Pitts, M. C., and Winker, D. M.: CALIPSO observations of stratospheric aerosols: a preliminary assessment, Atm. Chem.
    Phys., 7, 5283–5290, https://doi.org/10.5194/acp-7-5283-2007, 2007.

Tritscher, I., Pitts, M. C., Poole, L. R., Alexander, S. P., Cairo, F., Chipperfield, M. P., Groß, J.-U., Höpfner, M., Lambert, A., Luo, B.,
    Molleker, S., Orr, A., Salawitch, R., Snels, M., Spang, R., Woiwode, W., and Peter, T.: Polar stratospheric clouds: Satellite observations,
    processes, and role in ozone depletion, Rev. Geophys., 59, 1–81, https://doi.org/10.1029/2020RG000702, 2021.

Tsias, A., Wirth, M., Carslaw, K. S., Biele, J., Mehrtens, H., Reichardt, J., Wedekind, C., Weiß, V., Renger, W., Neuber, R., von Zahn, U.,
    Stein, B., Santacesaria, V., Stefanutti, L., Fierli, F., Bacmeister, J., and Peter, T.: Aircraft lidar observations of an enhanced type Ia polar
    stratospheric clouds during APE-POLECAT, J. Geophys. Res., 104, 23 961–23 969, https://doi.org/10.1029/1998JD100055, 1999.

Voelger, P. and Dalin, P.: A case study of a quasistationary, very long polar stratospheric cloud layer edge, J. Meteorol. Soc. Japan, 99,
    https://doi.org/doi.org/10.2151/jmsj.2021-025, 2021.

Voelger, P. and Nikulin, G.: The new lidar system at the Swedish Institute of Space Physics in Kiruna: Description and first measurements, in:
    Proceedings of the 17th ESA Symposium on European Rocket and Balloon Programmes and Related research, vol. SP-590, pp. 321–326,
    2005.

von der Gathen, P., Kivi, R., Wohltmann, I., Salawitch, R. J., and Rex, M.: Climate change favours large seasonal loss of Arctic ozone, Nat.
    Commun., 12, https://doi.org/10.1038/s41467-021-24089-6, 2021.